Original Paper

Causal Modeling to Mitigate Selection Bias and Unmeasured Confounding in Internet-Based Epidemiology of COVID-19: Model Development and Validation

Nathaniel Stockham[1], MSc; Peter Washington[2], PhD; Brianna Chrisman[2], PhD; Kelley Paskov[3], MSc; Jae-Yoon Jung[4], PhD; Dennis Paul Wall[4,5], PhD

[1]Neurosciences Interdepartmental Program, Stanford University, Palo Alto, CA, United States

[2]Department of Bioengineering, Stanford University, Stanford, CA, United States

[3]Biomedical Informatics Program, Stanford University, Stanford, CA, United States

[4]Department of Biomedical Data Science, Stanford University, Stanford, CA, United States

[5]Department of Pediatrics, Stanford University, Stanford, CA, United States

Corresponding Author:
Nathaniel Stockham, MSc
Neurosciences Interdepartmental Program
Stanford University
3145 Porter Dr
Palo Alto, CA, 94304
United States
Phone: 1 2056021832
Email: stockham@stanford.edu

Abstract

Background: Selection bias and unmeasured confounding are fundamental problems in epidemiology that threaten study internal and external validity. These phenomena are particularly dangerous in internet-based public health surveillance, where traditional mitigation and adjustment methods are inapplicable, unavailable, or out of date. Recent theoretical advances in causal modeling can mitigate these threats, but these innovations have not been widely deployed in the epidemiological community.

Objective: The purpose of our paper is to demonstrate the practical utility of causal modeling to both detect unmeasured confounding and selection bias and guide model selection to minimize bias. We implemented this approach in an applied epidemiological study of the COVID-19 cumulative infection rate in the New York City (NYC) spring 2020 epidemic.

Methods: We collected primary data from Qualtrics surveys of Amazon Mechanical Turk (MTurk) crowd workers residing in New Jersey and New York State across 2 sampling periods: April 11-14 and May 8-11, 2020. The surveys queried the subjects on household health status and demographic characteristics. We constructed a set of possible causal models of household infection and survey selection mechanisms and ranked them by compatibility with the collected survey data. The most compatible causal model was then used to estimate the cumulative infection rate in each survey period.

Results: There were 527 and 513 responses collected for the 2 periods, respectively. Response demographics were highly skewed toward a younger age in both survey periods. Despite the extremely strong relationship between age and COVID-19 symptoms, we recovered minimally biased estimates of the cumulative infection rate using only primary data and the most compatible causal model, with a relative bias of +3.8% and –1.9% from the reported cumulative infection rate for the first and second survey periods, respectively.

Conclusions: We successfully recovered accurate estimates of the cumulative infection rate from an internet-based crowdsourced sample despite considerable selection bias and unmeasured confounding in the primary data. This implementation demonstrates how simple applications of structural causal modeling can be effectively used to determine falsifiable model conditions, detect selection bias and confounding factors, and minimize estimate bias through model selection in a novel epidemiological context. As the disease and social dynamics of COVID-19 continue to evolve, public health surveillance protocols must continue to adapt; the emergence of Omicron variants and shift to at-home testing as recent challenges. Rigorous and transparent methods to develop, deploy, and diagnosis adapted surveillance protocols will be critical to their success.

(JMIR Public Health Surveill 2022;8(7):e31306) doi: 10.2196/31306

KEYWORDS

selection bias; COVID-19; epidemiology; causality; sensitivity analysis; public health; surveillance; method; epidemiologic research design; model; bias; development; validation; utility; implementation; sensitivity; design; research; epidemiology

Introduction

Accurate estimation of disease parameters is a fundamental problem in epidemiology. The internal and external validity of epidemiological studies is threatened by unmeasured confounding and selection bias [1,2]. There is an extensive and sophisticated literature focused on mitigating these threats by study design and poststudy statistical adjustment [3-5]. In particular, the randomization paradigm for treatment assignment and sample selection has served at the de facto standard for identifying causal effects and point estimates of disease parameters in a target population. However, even studies with perfect randomization can still suffer from unmeasured confounding and selection bias via a variety of phenomena, such as participant noncompliance, unit nonresponse, incomplete registers of the target population, and data collection failures [6]. In the past decade, there have been several advances in the theoretical treatment of these threats, particularly in the graphical causal modeling literature, where the problems of selection bias and unmeasured confounding have received a comprehensive theoretical treatment [7-9]. Although these recent methods provide a clear conceptual and mathematical framework, they have yet to be routinely deployed in the epidemiological community at large [10,11].

This gap is particularly acute in internet-based public health and surveillance. Internet-based sampling in general suffers from unknown selection mechanisms on largely unobservable and dynamic populations, making traditional adjustment methods that require external data about the target population vulnerable to model violation. Previous studies that augmented traditional surveillance mechanisms with internet-based data have proved highly successful at imputing missing or time-delayed information [12,13]. However, it is challenging to model emerging pathogens and adapt to changing internet user behavior across time and social context [14]. This fundamental difficulty was demonstrated vividly early in the COVID-19 pandemic as several highly sophisticated crowdsourced internet-based surveillance efforts were launched in response to the pandemic [15-21]. Despite explicit support by global social media and web service vendors, these early efforts yielded significantly biased estimates of key epidemiological parameters [22-26]. Internet-based epidemiology must adopt methodological approaches appropriate to the dynamic and unobservable features of internet populations.

In this work, we seek to address this gap between recent theoretical developments and the current practice of internet-based public health surveillance. We present structural causal modeling as a guide to epidemiological judgement through encoding epidemiological knowledge into models that can be tested using sample data, and we describe a general graphical method for deriving falsifiable model conditions. Importantly, this approach can be deployed using only the sampled data, whereas traditional methods for detecting confounding and selection bias require some information about the unsampled or missing data from units with partial data or external data, such as census or health care system medical records [1]. For novel and dynamic phenomena, the required external information may be unavailable, unreliable, or impractical to collect in the timespan available. Our objective is to demonstrate the practical utility of model diagnosis and selection using statistical criteria derived from structural causal models.

Methods

Structural Causal Models

Structured causal models permit the formal encoding of causal mechanisms and have been extended to formally analyze studies in the presence of selection bias and unmeasured confounding. The mathematical tool necessary for this work is d-separation on directed acyclic graphs (DAGs). Here, we briefly review d-separation notation and concepts. We can represent a probability distribution as a DAG where nodes represent variables X, Y, and Z and edges represent functional dependencies between variables. The formalism of d-separation is a mapping between the DAG of a probability distribution and the conditional independencies of that distribution; this is stated formally in the conditional independence statements of Figure 1. To state that variables X and Y are d-separated by Z is to state that X and Y are conditionally independent if conditioned on variable Z. Conversely, if X and Y are not d-separated by Z, then X and Y are conditionally dependent if conditioned on Z. A path in a DAG is a sequence of edges (regardless of direction), and every path can be decomposed into a sequence of path elements of edges, chains, forks, and colliders, as shown in Figure 1. The variables X and Y are d-separated in the DAG if all paths from X to Y in the graph are "blocked." Intuitively, a path from X to Y is blocked if no information about X can be inferred from observing Y via information transferred along that path.

The d-separation path element rules determine whether a path between X and Y is blocked. A path between X and Y can be blocked in 2 different ways by conditioning on a set of variables W. If the path contains a fork or a chain element, then it is blocked if the middle variable (Z in Figure 1) in at least 1 of the fork or chain elements is in W. If the path contains a collider element, then the path is blocked only if the middle variable is not in W. Conditioning on the middle variable of a collider element can unblock the path and make X and Y not d-separated. To illustrate this concept more explicitly, consider 2 independent binary 0,1 variables X and Y, where Z = X + Y. If we condition on Z such that Z=1, then X and Y would appear anticorrelated (nonindependent) because samples with X=Y=0 and X=Y=1 are, by definition, never observed in the subset where Z=1. This effect is known as *collider bias* and is a major source of selection bias in epidemiological studies. For further reading, there are several good introductions to d-separation in graphical models [6,9].

Figure 1. Conditional independence statements and d-separation rules.

Conditional independence statements:

$$\begin{array}{ll} X,Y \text{ d-separated by } Z: & (X \perp\!\!\!\perp Y|Z) \iff P(X,Y|Z)=P(X|Z)P(Y|Z) \\ X,Y \text{ not d-separated by } Z: & (X \not\!\perp\!\!\!\perp Y|Z) \iff P(X,Y|Z)\neq P(X|Z)P(Y|Z) \end{array}$$

Path element rules:

$$\begin{array}{rll} \text{Edge}: X \rightarrow Y & \iff (X \not\!\perp\!\!\!\perp Y) & \\ \text{Chain}: X \rightarrow Z \rightarrow Y & \iff (X \not\!\perp\!\!\!\perp Y), (X \perp\!\!\!\perp Y|Z) & : \text{blocked by } Z \\ \text{Fork}: X \leftarrow Z \rightarrow Y & \iff (X \not\!\perp\!\!\!\perp Y), (X \perp\!\!\!\perp Y|Z) & : \text{blocked by } Z \\ \text{Collider}: X \rightarrow Z \leftarrow Y & \iff (X \perp\!\!\!\perp Y), (X \not\!\perp\!\!\!\perp Y|Z) & : \text{unblocked by } Z \end{array}$$

The only additional conceptual step necessary for analyzing selection bias is to add the sampling mechanism to the initial causal graph G to create the augmented causal graph G_s. The encoded sampling mechanism determines the value of the sampling indicator variable S, where S=1 if the unit was sampled and S=0 otherwise. Additionally, any mechanism that filters data after primary collection induces an additional selection bias and must also be encoded in G_s. The augmented graph G_s obeys d-separation rules, but for clarity, the sampling indicator S node is depicted in G_s with a double ring to emphasize that S=1 for all samples by definition; all d-separation statements in G_s must be evaluated conditional on S=1.

For any graph G_s, the s-recoverability condition states that for any variables Y and X in G_s, the distribution of the sample P(Y|X,S=1) is identical to the distribution of the target population P(Y|X) if and only if Y and S are d-separated by X [8]. Assuming the graph is faithful, S and Y conditioned on X are independent if and only if there is no selection bias or unmeasured confounding. It is not possible to directly test for independence between S and Y using sample data, because is no variation as S=1 by definition, but other surrogate variables in the sample data can be used to test independence of S and Y.

We demonstrate this principle in Figure 2 using the causal graphs $G_{A,s}$, $G_{B,s}$, $G_{C,s}$, and $G_{D,s}$ with outcome variable Y, instrumental variable V on variable X relative to Y, and a sample indicator variable S determined by X. Here we define an instrumental variable V on X relative to Y as a variable V that is not independent of X (V and X not d-separated), but V is independent of Y conditional on X (V and Y are d-separated by X). In graph $G_{A,s}$, the variables V and Y are trivially d-separated (d-separated without any blocking variables) and therefore independent. If there is any selection bias ($G_{B,s}$, $G_{C,s}$) or unmeasured confounding ($G_{D,s}$), then V and Y are not trivially d-separable and are not independent. For example, suppose the null hypothesis of statistical independence between V and Y is rejected in the sampled data. Then the graph $G_{A,s}$ is not compatible with the sample data, but alternative graphs $G_{C,s}$, $G_{B,s}$, and $G_{D,s}$ are compatible with nonindependent V and Y and should be considered. Any augmented causal graph G_s entails a set of conditional independencies that can be statistically tested using only the sample data. For more complex graphs, there are several software tools that will compute all the entailed independencies, of which *dagitty* is perhaps the most user friendly [26].

In this work, we focus on graphical modeling as a formalism to aid epidemiological judgment. Epidemiological knowledge tightly constrains the set of possible explanatory scenarios for a given context; the difficulty is choosing which of these scenarios is most plausible. Statistically testing the independencies implied by the causal graph encoding is a direct method to select between scenarios. We now demonstrate this approach in an applied problem of estimating the cumulative infection rate CI_P of SARS-CoV-2 in the COVID-19 New York City (NYC) spring 2020 epidemic through a prospectively collected crowdsourced internet survey.

Figure 2. Example causal graphs with selection bias and unmeasured confounding.

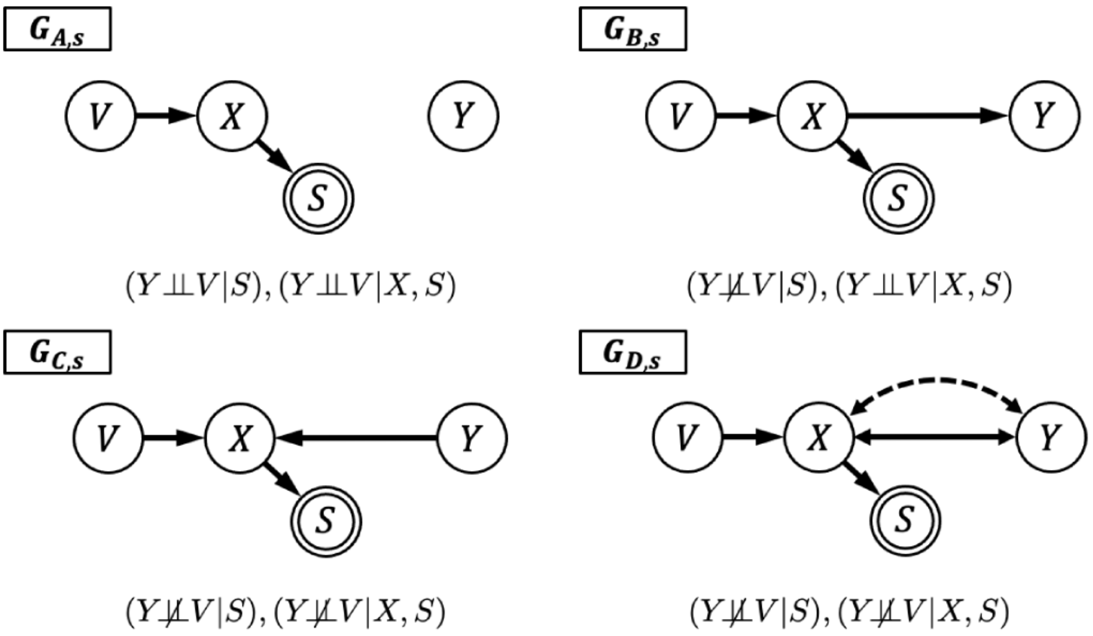
$G_{A,s}$
V
X
Y
S
$(Y \perp\!\!\!\perp V|S), (Y \perp\!\!\!\perp V|X,S)$
$G_{B,s}$
V
X
Y
S
$(Y \not\perp\!\!\!\perp V|S), (Y \perp\!\!\!\perp V|X,S)$
$G_{C,s}$
V
X
Y
S
$(Y \not\perp\!\!\!\perp V|S), (Y \not\perp\!\!\!\perp V|X,S)$
$G_{D,s}$
V
X
Y
S
$(Y \not\perp\!\!\!\perp V|S), (Y \not\perp\!\!\!\perp V|X,S)$

Recruitment

Initial crowdsourced epidemiology efforts in the COVID-19 pandemic focused on surveys collected from a variety of internet sources and target populations. Instead of recruiting via major internet platforms such as Facebook and Google, we recruited our survey participants from the Amazon Mechanical Turk (MTurk) crowdworking platform. MTurk is an internet-based labor market where a research group or business (*requesters*) can create and disseminate a human intelligence task (HIT) to a distributed human labor pool (*workers*) that can accept and complete these tasks for a known monetary reward upon satisfactory completion of the task. A HIT can range from transcribing an audio file to a personality survey, and requesters can restrict the task workers within a specific geographic area or demographic subset. All MTurk workers in the United States are adults of age 18 years or older.

We chose the MTurk population for 2 reasons. First, MTurk has been successfully used by many academic groups, including our own, across a broad array of disciplines [27-32]. Second, the demographics and health status of the MTurk worker population in the United States has been repeatedly characterized and has remained stable through time, closely matching the racial and ethnic composition of the United States but skewing toward women, a younger age, worse mental health, and lower income than the US population [28]. Any MTurk worker registered as residing in New York State or New Jersey was permitted to respond to the survey via the MTurk HIT job posting with restriction that a worker could respond only once per survey period. No other restrictions or invitation mechanisms were used in either survey period.

Human Subject Research Ethical Statement

This research was not found to be considered human subject research as the survey did not collect any personally identifying information or set of information that could be reidentifying, in compliance with MTurk's policy prohibiting any transmission of workers' personally identifiable information to requesters and Stanford University research policy GUI-H12. Research was carried out in a way that followed ethical guidelines set by the Declaration of Helsinki. All MTurk tasks are carefully reviewed before being posted, and MTurk workers are able to accept but then refuse to complete any task or any part of a task at any point in time. Furthermore, the survey task included an introduction page that informed the respondents of the purpose and content of this survey and for what purposes their response data would be used.

Overview of Survey Design

We collected primary data from the MTurk population listed as currently residing in New Jersey or New York. Data for surveys s_1 and s_2 were collected in 2 successive periods: April 11-14 and May 8-11, 2020. During this period, both New York and New Jersey were under a statewide stay-at-home order that greatly restricted travel and prohibited public gatherings [33,34]. We collected primary data from 2 survey periods to estimate the trajectory of the spring 2020 COVID-19 epidemic in NYC and assess the stability of model selection across 2 different phases of the epidemic. The context of NYC in spring 2020 was chosen because it was 1 of the first major COVID-19 epidemics. A Qualtrics survey was created for each survey run, with a reward (median completion time) for the surveys of US $1 (5 minutes) and US $1.25 (6 minutes) for s_1 and s_2, respectively. This reward is consistent with other MTurk HITs for the time required. Before accepting the task, the participant was aware of the overall survey subject (COVID-19) and the monetary reward for completion. We excluded responses from participants that were incomplete or out-of-area, as determined by geolocation information provided by Qualtrics. The included responses were split by collection period and aggregated into 3 nested geographic areas: New Jersey and New York (NJ/NY), the section of the New York City Combined Statistical Area contained within New Jersey and New York (NYC CBSA), and NYC proper.

Before answering any questions, the survey asked each participant (respondent) to privately list their 5 closest peer relationships (relations) with whom they typically socialize in person. There was large variation in the number of contacts for each person during the mandatory stay-at-home orders. Instead of asking respondents about their total number of contacts, we asked about their closest peer relationships because these are the set of persons whose current health status and household characteristics would most likely be known to the respondents. Furthermore, we only asked about 5 relations to minimize the time to complete the survey. The survey queried each respondent about the demographic, employment characteristics, and possible COVID-19 symptoms of both themselves and their relations. The survey also queried each respondent about both their household and their relations' households, including household size and whether any member had a confirmed SARS-CoV-2 infection since March 15, 2020. These questions were chosen to permit comparison of respondents and relations to known census demographic data and to estimate the cumulative number of infected households and individuals within a specified geographic area. The survey material is included in Multimedia Appendices 1 and 2.

Statistical Analysis

Estimator Definition

We defined a household-based cumulative infection rate estimator $\widehat{CI}_{P_S}$ on a sample P_S for the cumulative infection rate as:

$$CI_P = \frac{1}{N_P}\sum_{p\in P} C_p$$

where C_p is an indicator variable for the confirmed SARS-CoV-2 infection status of person p in a population P of size N_P. We defined the household secondary attack rate (SAR_h) as the ratio of secondary household cases to the total population of exposed household members. We can write SAR_h formally as:

$$SAR_h = \frac{\sum_{h\in H} C_h((\sum_{p\in h} C_p)-1)}{\sum_{h\in H} C_h(N_h-1)}$$

where H is the set of unique households in population P, indicator variable C_h=1 for if there is at least 1 SARS-CoV-2 infection in household h, and N_h the size of household h in H. Let the total population be defined as the sum of the household members N_P=$\Sigma_{h\varepsilon H}$ N_h. We can then rewrite CI_P in terms of households as:

$$CI_P = \frac{1}{N_P}\sum_{h\in H}\sum_{p\in h} C_p = \frac{1}{N_P}\sum_{h\in H} C_h\cdot(1+SAR_h(N_h-1))$$

We then defined the estimator $\widehat{CI}_{P_S}$ of CI_P on a sample P_S as:

$$\widehat{CI}_{P_S} = \frac{1}{N_{P_S}}\sum_{h\in H_S} C_h\cdot(1+SAR_h(N_h-1))$$

with unique households H_S. The estimator $\widehat{CI}_{P_S}$ is consistent as H_S goes to H if P(C_h, N_h|h in H_s)=P(C_h, N_h) of the target population. In the special case of SAR_h=0, $\widehat{CI}_{P_S}$ is an unbiased estimator of the cumulative household infection rate CI_H under the less restrictive condition of P(C_h|S=1)=P(C_h).

Structural Causal Models

The survey data were modeled in a causal graph encoding the variables and assumptions, as depicted in Figure 3. Every person in the population P was assigned 2 indicator variables Res_i and Rel_{ij} and the outcome variables $C_{h,Res,i}$ and $C_{h,Rel,ij}$. The variable Res_i=1 if person p_i is a respondent to the survey, and Rel_{ij}=1 if p_i in P would choose person p_j as a relation in the context of this survey. In the sample, the set of respondents is $P_{S,Res}$={p_i|Res_i=1}, the set of relations is $P_{S,Rel}$={p_j|Rel_{ij}=1, p_i in $P_{S,Res}$}, and the total sample is P_S=$P_{S,Res}$ ∪ $P_{S,Rel}$. The outcome variable $C_{h,Res,i}$=1 if there is at least 1 confirmed SARS-CoV-2 infection in the household of respondent p_i in $P_{S,Res}$, and $C_{h,Rel,ij}$=1 if there is at least 1 confirmed infection in the household of relation p_j in $P_{S,Rel}$. For each response, there is 1 respondent and 5 relations chosen by that respondent. In the causal graphs in Figure 3, the subgraph that includes variables pertaining to relations is replicated identically for all 5 relations. Given that this was an anonymous internet survey, we assumed no information bias due to intentional misrepresentations on the part of the respondents or relations. We also assumed there was no information bias due to testing constraints at the level of the household.

We defined 4 possible causal models depicted in Figure 3, augmented with the sampling indicator variable S. All variables were conditioned on a common geographic area, which was suppressed in the graphs and notation for clarity.

The first 3 causal models $G_{Res,s}$, $G_{Rel,s}$, and $G_{All,s}$ all shared the same causal graph, as represented in the first graph in Figure 3, and differed only in terms of the data used. The first causal graph encoded that the age variable A of a person influences whether they respond as a relation/respondent in variable R, which in turn determines whether they are in the sample S. Furthermore, the household infection status C_h of the person was assumed to be unrelated to the other variables. The first causal model $G_{Res,s}$ only used data on respondents, whereas the second model $G_{Rel,s}$ only used data on relations. The third model $G_{All,s}$ combined respondents' and relations' data.

Figure 3. Alternative causal graphs.

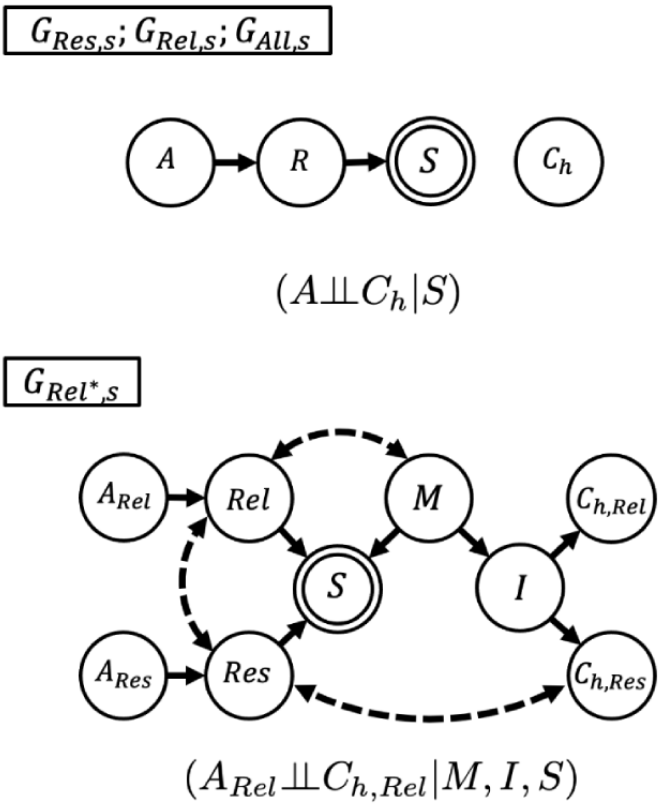
$G_{Res,s}; G_{Rel,s}; G_{All,s}$
A
R
S
C_h
$(A \perp\!\!\!\perp C_h | S)$
$G_{Rel^*,s}$
A_{Rel}
Rel
M
$C_{h,Rel}$
S
I
A_{Res}
Res
$C_{h,Res}$
$(A_{Rel} \perp\!\!\!\perp C_{h,Rel} | M, I, S)$

The second graph in Figure 3 corresponds to the fourth causal model $G_{Rel*,s}$, which encoded a possible confounding between S and C_{Res} and between S and C_{Rel}. In particular, $G_{Rel*,s}$ modeled the case where the respondents' household status $C_{h,Res}$ is related to the relations' household status $C_{h,Rel}$ through a transmission event I between a respondent and a relation due to the recent close contact event M. The variables I and M d-separated the sampling indicator S and the outcome of interest $C_{h,Rel}$, but the infection event I was unobservable. However, if we filtered the samples so that M=0 (excluding relations with close contact events with the respondent), then I=0 for the retained samples because there can be no transmission without close contact; filtering on M=0 effectively conditioned on M=0 and I=0. Filtering on M also induced another selection bias modeled by the edge M to S, but S and $C_{h,Rel}$ remained d-separated as did $C_{h,Rel}$ and A_{Rel}. Therefore, the graph $G_{Rel*,s}$ implied that $P(C_{h,Rel}|M=0,I=0,S=1)=P(C_h)$ and furthermore implied that $C_{h,Rel}$ and A_{Rel} are statistically independent. Effectively, this model excluded information from respondents and excluded relations that had recent in-person contact with the respondents. Practically, this model reduced overestimation of the cumulative infection rate due to possible common causes of the infection status of respondents and relations, such as when a respondent transmits an infection to a relation.

These 4 models can be compared and ranked empirically by statistical tests of the conditional independences implied by their d-separation conditions. Each causal model in Figure 3 has at least 1 independence statement that is testable using the observed data on the age and household infection status of the respondents and relations. From 1 statistical test of the independence statement, we can distinguish which causal model is compatible with the data for each survey period using only the survey sample data. This is an important methodological point, given that the current practice for model diagnosis and selection assumes strong prior knowledge about the target population on several demographic variables. No external data are required for this type of diagnostic analysis, which is a key advantage when the target population is unstudied, inaccessible, or dynamic through time.

We evaluated the causal models by statistically testing the implied independence of A; C_h in models $G_{Res,s}$, $G_{Rel,s}$, and $G_{All,s}$; and A_{Rel} and $C_{h,Rel}$ in model $G_{Rel*,s}$ using the Fisher exact test for independence. For each model, we filtered the data, as specified in the model, median-split the age variable, and performed Fisher exact tests on the 2×2 table of the age group (A_0, A_1) by house infection status ($C_{h,0}$, $C_{h,1}$) with point test statistics shown in Table 1. Ages for respondents and relations were randomly assigned within the recorded 5-year bin across independent replications (n=1000). The median odds ratio with 95% CIs and median *P* values are reported in Table 1.

Table 1. Model selection by conditional independence tests.

Survey	Odds ratio (95% CI)	*P* value	Sample size, N
$G_{Res,s}$			
s_1	0.802 (0.765-0.922)	.77	527
s_2	0.271 (0.202-0.438)	.01	513
$G_{Rel,s}$			
s_1	0.955 (0.885-1.026)	.90	2635
s_2	0.634 (0.581-0.694)	.01	2565
$G_{All,s}$			
s_1	0.919 (0.824-1.007)	.73	3162
s_2	0.572 (0.525-0.614)	<.001	3078
$G_{Rel*,s}$			
s_1	0.977 (0.855-1.130)	.99	1340
s_2	1.472 (1.216-1.823)	.28	1104

In the general case, there will be no ground truth to compare the model against. However, in this study, we assessed the model performance directly. Due to the particular conditions of the NYC epidemic, the performance of the $\widehat{CI}_{P_S}$ estimator in each causal model can be evaluated directly from the CI_P reported by the New Jersey and New York State health departments. Under the test rationing and home quarantine policies of New York and New Jersey during the spring 2020 epidemic, diagnostic real-time reverse transcription polymerase chain reaction (rRT-PCR) SARS-CoV-2 tests were restricted to individuals hospitalized with COVID-19 symptoms. Households with a member who tested positive were required by law to quarantine [35-40]. Although multiple members of a given household might have SARS-CoV-2 infections, no additional rRT-PCR tests would be performed on other household members unless they were hospitalized. Therefore, the reported CI_P is as if SAR_h=0 where no secondary household cases are reported. We aggregated confirmed SARS-CoV-2 infections as reported by the New York and New Jersey governments for each date and geographic area (NJ/NY, NYC CBSA, NYC) and calculated the CI_P relative to the American Community Survey (ACS) population for each. To evaluate the performance of each model, we computed the cumulative infection rate estimator $\widehat{CI}_{P_S}$ at SAR_h=0 and calculated its relative bias from the reported CI_P for each area and period.

To demonstrate the practical epidemiological utility of this type of internet-based sampling, we calculated $\widehat{CI}_{P_S}$ for different values of SAR_h using the causal model most compatible with the primary data, deriving 95% CIs by bootstrap resampling (n=1000).

Results

Demographics

In total, 527 and 513 responses met the inclusion criteria from surveys s_1 and s_2, respectively. Demographic information is summarized as frequencies for each collection period, with Pearson chi-squared tests performed to compare raw counts to demographic distributions in the 2018 ACS update of the US Census Bureau (Table 2).

Significant age skews were apparent across all survey periods, with both respondents and relations skewing significantly younger than the known population distribution, while sex distributions were not significantly different than the ACS estimate for New York and New Jersey. This large age skew made the sample highly unrepresentative of the target population, but with a correctly specified causal model, it was possible to obtain an unbiased estimate of the cumulative infection rate CI_P, as we next demonstrate through model diagnosis, selection, and evaluation.

Table 2. Demographic characteristics of survey samples.

Characteristics	Respondents, n(%)		Relations, n(%)		Combined, n(%)		ACS[a] (%)
	Survey s_1 (N=527)	Survey s_2 (N=513)	Survey s_1 (N=2635)	Survey s_2 (N=2565)	Survey s_1 (N=3162)	Survey s_2 (N=3078)	
Age (years)							
<19	2 (0.4)	5 (1.0)	264 (10.0)	356 (13.9)	266 (8.4)	361 (11.7)	22.7
19-29	184 (34.9)	192 (37.4)	620 (23.5)	575 (22.4)	804 (25.4)	767 (24.9)	15.2
30-39	170 (32.3)	163 (31.8)	531 (20.2)	525 (20.5)	701 (22.2)	688 (22.4)	13.2
40-49	89 (16.9)	77 (15)	400 (15.2)	344 (13.4)	489 (15.5)	421 (13.7)	12.9
50-59	56 (10.6)	46 (9.0)	367 (13.9)	346 (13.5)	423 (13.4)	392 (12.7)	14.1
60-69	19 (3.6)	24 (4.7)	284 (10.8)	294 (11.5)	303 (9.6)	318 (10.3)	11.2
≥70	7 (1.3)	6 (1.2)	169 (6.4)	125 (4.9)	176 (5.6)	131 (4.3)	10.6
Chi-square (*df*=6)	475	480	457	358	793	672	N/A[b]
P value	<.001	<.001	<.001	<.001	<.001	<.001	N/A
Sex[c]							
N/A	1 (0.2)	3 (0.6)	20 (0.8)	77 (3.0)	21 (0.7)	80 (2.6)	N/A
Female	267 (50.7)	286 (55.8)	1353 (51.3)	1303 (50.8)	1620 (51.2)	1589 (51.6)	51.4
Male	259 (49.1)	224 (43.7)	1262 (47.9)	1185 (46.2)	1521 (48.1)	1409 (45.8)	48.6
Chi-square (*df*=1)	0.08	4.50	0.13	0.97	0.046	3.14	N/A
P value	.77	.03	.71	.32	.83	.07	N/A
Occupation (multiple)							
Essential worker	153 (30.0)	140 (27.9)	N/A	N/A	N/A	N/A	N/A
Food service	31 (5.9)	27 (5.3)	N/A	N/A	N/A	N/A	N/A
Health care	66 (12.5)	69 (13.5)	N/A	N/A	N/A	N/A	N/A
Work from home	152 (28.8)	183 (35.7)	N/A	N/A	N/A	N/A	N/A
Not working	71 (13.5)	86 (16.8)	N/A	N/A	N/A	N/A	N/A
Other	231 (43.8)	173 (33.7)	N/A	N/A	N/A	N/A	N/A

[a] ACS: American Community Survey of the US Census Bureau.

[b] N/A: not applicable.

[c] Sex inferred from the reported gender identity for comparison with the ACS.

Model Diagnosis, Selection, and Evaluation

In the first survey period, no model could be rejected at nominal α=0.05, but in the second survey period, only model $G_{Rel*,s}$ could not be rejected. The most likely explanation for why the 4 models were more distinguished in the second period is that the cumulative infection rate increased through the course of the epidemic, giving greater power to detect a statistical dependence in a model, even though the total sample size was similar between periods for each model.

Model Performance

The model $G_{Rel*,s}$ recovered accurate cumulative infection rate $\widehat{CI}_{Ps}$ estimates, with the lowest bias across both survey periods for the full sample (NJ/NY), as displayed in Figure 4, with the estimator variance for all models increasing as the sample size decreased with a smaller geographic area.

Figure 4. Relative bias of cumulative infection estimates by geographic area, model, and survey period. NJ/NY: New Jersey and New York; NYC: New York City; NYC CBSA: New York City Combined Statistical Area contained within New Jersey and New York.

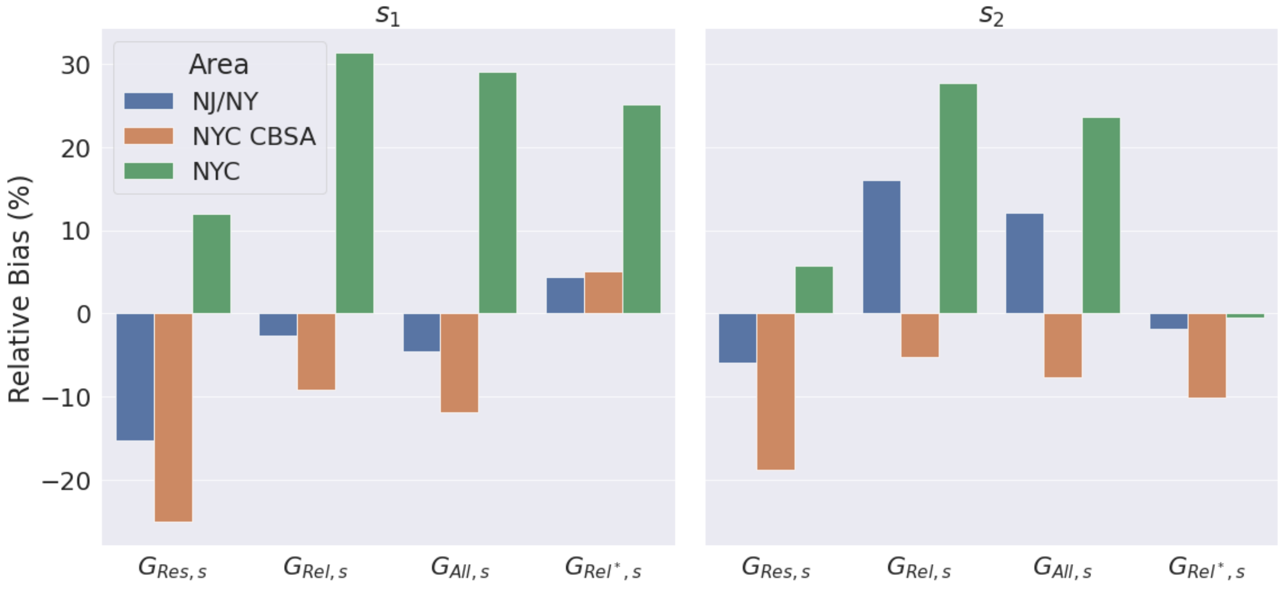

Estimating the Cumulative Infection Rate from the Household Secondary Attack Rate

The model $G_{Rel*,s}$ was used to calculate the cumulative infection rate estimator $\widehat{CI}_{P_s}$ for different values of SAR_h, as displayed in Figure 5. For all geographic areas and survey periods, the median $\widehat{CI}_{P_s}$ estimate was approximately 1-4 times higher than the reported cumulative infection rate CI_P, with upper bounds ranging from 2.5-5 times higher.

Figure 5. Estimated cumulative infection rate by geographic area, household secondary attack rate (SARh), and survey period. Dashed lines are the reported CI_p for the survey period, color-matched to the geographic area. NJ/NY: New Jersey and New York; NYC: New York City; NYC CBSA: New York City Combined Statistical Area contained within New Jersey and New York.

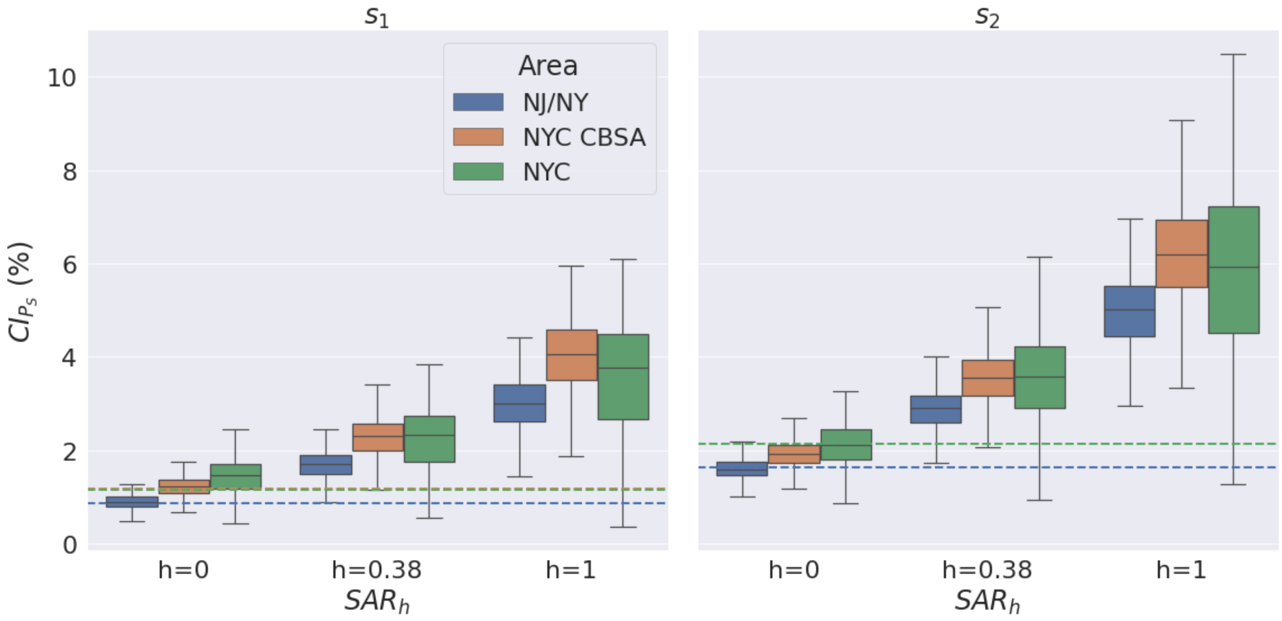

Reported Symptoms Among Respondents and Relations

The number of households with at least 1 confirmed SARS-CoV-2 infection increased by 2 times, and the number of households with at least 1 member recently hospitalized for influenza-like illness (hospital ILI) increased by 1.5 times for both respondents and relations across the 2 survey periods, as shown in Table 3. Despite this, the marginal rates of common symptoms (fever, aches, anosmia, allergy) remained similar across both periods. This highlights the practical difficulties of estimating changes in CI_P by using common symptom checklists, as reported by internet surveys.

The correlation between health status indicators and symptoms remained largely the same across both periods (Figure 6). The notable exception is that the correlation between SARS-CoV-2 and hospital ILI increased from the first to the second survey period, presumably corresponding to the conversion from diagnosis to hospitalization as the epidemic progressed.

Table 3. Respondent/relation household heath status and symptoms by survey period.

Person	Household health status, n (%)		Reported symptoms, n (%)			
	SARS-CoV-2[a]	Hospital ILI[b,c]	Fever	Aches	Anosmia	Allergy
Survey s_1						
Respondents (N=1040)	25 (2.4)	24 (2.3)	32 (3.1)	112 (10.8)	45 (4.3)	89 (8.6)
Relations (N=5200)	155 (3.0)	109 (2.1)	211 (4.1)	325 (6.3)	167 (3.2)	226 (4.4)
Survey s_2						
Respondents (N=1040)	53 (5.2)	33 (3.2)	23 (2.3)	145 (14.3)	46 (4.5)	104 (10.2)
Relations (N=5200)	295 (5.8)	169 (3.3)	154 (3.0)	337 (6.6)	180 (3.6)	192 (3.8)

[a] SARS-CoV-2: at least 1 household member had tested positive for SARS-CoV-2 infection by real-time reverse transcription polymerase chain reaction (rRT-PCR).

[b] ILI: influenza-like illness.

[c] Hospital ILI: at least 1 household member was recently hospitalized for an ILI.

Figure 6. Reported symptom correlations by survey period. SARS-CoV-2 : at least 1 household member tested positive for SARS-CoV-2 infection by rRT-PCR. Hospital ILI: at least 1 household member was recently hospitalized for an ILI. ILI: influenza-like illness; rRT-PCR: real-time reverse transcription polymerase chain reaction.

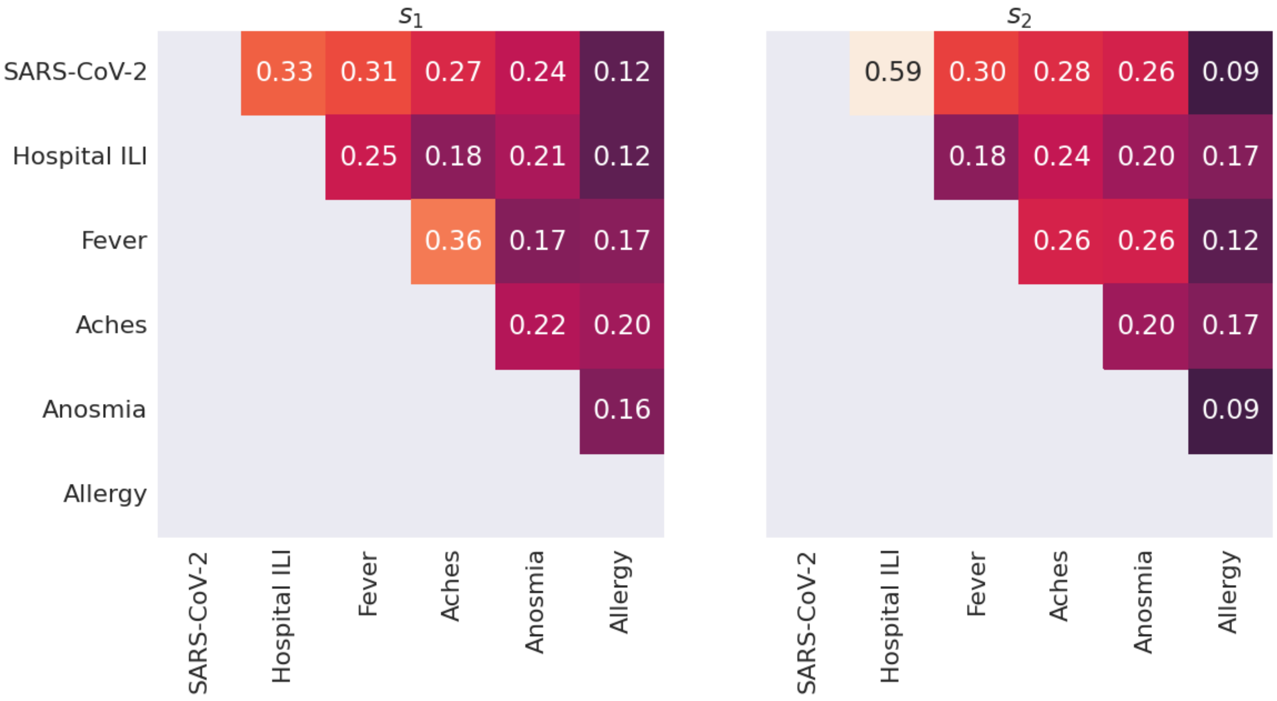

Discussion

Principle Findings

Using no external data and standard statistical independence tests, we were able to rank and reject all alternative models except the model $G_{Rel*,s}$ that yielded the lowest bias for the cumulative infection rate estimator $\widehat{CI}_{P_S}$, with a bias of less than 4% on the full sample despite the high skew toward younger ages relative to the target population. Without randomization or representativeness, this study recovered accurate estimates of a key epidemiological parameter using an internet-based crowdsourced population in a dynamic public health crisis using only a few hundred samples.

Although we primarily intend this work to demonstrate the broad utility of graphical models as an aid to epidemiologists, it is worth noting how useful internet-based epidemiology could prove in future epidemics by inspecting the estimates of $\widehat{CI}_{P_S}$ for varying SAR_h (Figure 5). A major source of confusion in the early COVID-19 pandemic was diverging estimates of the cumulative infection rate. By July 27, 2020, there were 228,679 rRT-PCR cumulative confirmed infections in NYC for a reported CI_P of 2.65%. However, the actual CI_P was estimated to be 23.3% by seroprevalence studies in the July 27-August 13, 2020, period—8.8 times higher [41-44]. A similar difference would imply that the reported CI_P of 2.14% by May 8, 2020, corresponded to an actual CI_P of ~19%. Using the simple method of estimating $\widehat{CI}_{P_S}$ by SAR_h=0.38, it would yield intermediate estimates implying upper bounds on the actual CI_P of 2.5 and 5 times the reported cumulative infection rate CI_P.

Limitations

The limitations of this approach are encoded directly in the set of causal graphs and entail explicit conditions where statistical tests will fail to reject incorrect models. For example, if age is a poor instrumental variable for response status, then with finite data, none of the models may be rejected by statistical tests. In contrast, if age is strongly related to the outcome variable household status C_h, but not response status, then all models could be rejected, even if there was no selection bias on C_h. More generally, if there is any relationship between a set of variables, there will be a statistically significant correlation, given sufficient data; therefore, any causal model regardless of its utility will be rejected if statistical tests are applied naively.

These inherent limitations are why we emphasize structural causal models as an aid and not a substitute for epidemiological judgment. The utility of causal modeling is the formal comparison and communication of alternative explanations of the sampled data. For example, in this study, we chose to not model information bias, instead focusing on detecting selection bias. The choice to ignore information bias is explicit in the presented causal graphs; none of them have a subgraph that models an information bias mechanism, such as rRT-PCR test constraints or inaccurate self-reporting. These causal models were constructed with these assumptions for the context and objectives of this study, and similar assumptions may not be acceptable for a different context or objective. The key point is that all these assumptions are made apparent on inspection of the causal graphs.

Conclusion

The COVID-19 pandemic is an unprecedented event, pushing the limits of the health care system worldwide. Reducing transmission via nonpharmacological interventions has been effective but requires near-real-time and accurate information across all segments of society, information that has been difficult to reliably ascertain. Given the vast divergence of cumulative infection rate estimates across early studies [43] and the consequences for undermining public trust, there is a clear use case for internet-based public health surveillance to rapidly estimate key epidemiological parameters. A major use of internet-based surveys in the COVID-19 pandemic has been estimating the rate of vaccine uptake. The Census Household Pulse and Delphi-Facebook overestimated COVID-19 vaccine uptake to May 2021 by 14% and 17%, respectively, in the United States [44], while a much smaller Axios-Ipsos online survey of a different design overestimated uptake by only 5% in the United States. Internet-based surveys are an important tool with several uses for managing a pandemic, but current methodology is hampered by an inability to successfully detect and mitigate estimate bias. However, looking beyond vaccine uptake, near-term public health interventions, and advances in treatments, COVID-19 continues to evolve along with human societies. Surveillance systems and statistical models that assume centralized reporting may not be as useful with the mass adoption of at-home tests for COVID-19; alternative approaches, such as the social network polling design used in this work, may need to be deployed. For these reasons, we hope that these recent advances in causal modeling theory are adopted by the epidemiological community for current and future epidemics.

Acknowledgments

Design, implementation, analysis, and preparation of the manuscript were performed by NS. We gratefully acknowledge conceptual input and constructive feedback from PW, BC, KP, JYJ, and DPW.

The work was supported in part by funds to DPW from the National Institutes of Health (1R01EB025025-01, 1R01LM013364-01, 1R21HD091500-01, 1R01LM013083); the National Science Foundation (Award 2014232), the Hartwell Foundation, the Bill and Melinda Gates Foundation, the Coulter Foundation, the Lucile Packard Foundation, Auxiliaries Endowment, the Islamic Development Bank (ISDB) Transform Fund, and the Weston Havens Foundation; program grants from Stanford University's Human Centered Artificial Intelligence Program, the Precision Health and Integrated Diagnostics Center, the Beckman Center, Bio-X Center, the Predictives and Diagnostics Accelerator, Spectrum, the Spark Program in Translational Research, and MediaX; and program grants from the Wu Tsai Neurosciences Institute's Neuroscience:Translate Program. We also acknowledge generous support from David Orr, Imma Calvo, Bobby Dekesyer, and Peter Sullivan. PW would like to acknowledge support from Mr. Schroeder and the Stanford Interdisciplinary Graduate Fellowship (SIGF) as the Schroeder Family Goldman Sachs Graduate Fellow.

Data Availability

The data underlying this paper will be shared upon reasonable request to the corresponding author.

Conflicts of Interest

None declared.

Multimedia Appendix 1

Survey materials for survey period 1.
[PDF File (Adobe PDF File), 133 KB-Multimedia Appendix 1]

Multimedia Appendix 2

Survey materials for survey period 2.
[PDF File (Adobe PDF File), 154 KB-Multimedia Appendix 2]

References

1. Smith LH. Selection mechanisms and their consequences: understanding and addressing selection bias. Curr Epidemiol Rep 2020 Aug 09;7(4):179-189. [doi: 10.1007/s40471-020-00241-6]
2. Hernán MA, Hernández-Díaz S, Robins JM. A structural approach to selection bias. Epidemiology 2004 Sep;15(5):615-625. [doi: 10.1097/01.ede.0000135174.63482.43] [Medline: 15308962]
3. Pearl J. Causality. 2nd ed. New York, NY: Cambridge University Press; 2009.
4. Bareinboim E, Pearl J. Causal inference and the data-fusion problem. Proc Natl Acad Sci U S A 2016 Jul 05;113(27):7345-7352 [FREE Full text] [doi: 10.1073/pnas.1510507113] [Medline: 27382148]
5. Richardson T, Robins J. A Unification of the Counterfactual and Graphical Approaches to Causality. Working Paper. Single World Intervention Graphs (SWIGs). URL: https://csss.uw.edu/files/working-papers/2013/wp128.pdf [accessed 2022-02-26]
6. Schuessler J, Selb P. Graphical causal models for survey inference. SocArXiv 2019:26. [doi: 10.31235/osf.io/hbg3m]
7. Saadati M, Tian J. Adjustment criteria for recovering causal effects from missing data. 2019 Presented at: Machine Learning and Knowledge Discovery in Databases: European Conference, ECML PKDD; September 16–20, 2019; Würzburg, Germany p. 561-577. [doi: 10.1007/978-3-030-46150-8_33]
8. Bareinboim E, Tian J, Pearl J. Recovering from selection bias in causal and statistical inference. 2014 Presented at: The 28th AAAI Conference on Artificial Intelligence; July 27–31, 2014; Québec City, Québec, Canada. [doi: 10.1609/aaai.v28i1.9074]
9. Hernán MA, Robins JM. Causal Inference: What If. URL: https://cdn1.sph.harvard.edu/wp-content/uploads/sites/1268/2021/03/ciwhatif_hernanrobins_30mar21.pdf [accessed 2022-02-26]
10. Pearce N, Lawlor DA. Causal inference: so much more than statistics. Int J Epidemiol 2016 Dec 01;45(6):1895-1903 [FREE Full text] [doi: 10.1093/ije/dyw328] [Medline: 28204514]
11. Petersen JM, Ranker LR, Barnard-Mayers R, MacLehose RF, Fox MP. A systematic review of quantitative bias analysis applied to epidemiological research. Int J Epidemiol 2021 Nov 10;50(5):1708-1730. [doi: 10.1093/ije/dyab061] [Medline: 33880532]
12. McGough SF, Brownstein JS, Hawkins JB, Santillana M. Forecasting Zika incidence in the 2016 Latin America outbreak combining traditional disease surveillance with search, social media, and news report data. PLoS Negl Trop Dis 2017 Jan;11(1):e0005295 [FREE Full text] [doi: 10.1371/journal.pntd.0005295] [Medline: 28085877]
13. Yang S, Santillana M, Kou SC. Accurate estimation of influenza epidemics using Google search data via ARGO. Proc Natl Acad Sci U S A 2015 Nov 24;112(47):14473-14478 [FREE Full text] [doi: 10.1073/pnas.1515373112] [Medline: 26553980]
14. Aiken EL, McGough SF, Majumder MS, Wachtel G, Nguyen AT, Viboud C, et al. Real-time estimation of disease activity in emerging outbreaks using internet search information. PLoS Comput Biol 2020 Aug;16(8):e1008117 [FREE Full text] [doi: 10.1371/journal.pcbi.1008117] [Medline: 32804932]
15. Carnegie Mellon University Delphi Research Group. COVIDcast. URL: https://delphi.cmu.edu/covidcast [accessed 2022-02-26]
16. Facebook. Symptoms Map and Dashboard. URL: https://dataforgood.facebook.com/covid-survey [accessed 2022-02-26]
17. Menni C, Valdes AM, Freidin MB, Sudre CH, Nguyen LH, Drew DA, et al. Real-time tracking of self-reported symptoms to predict potential COVID-19. Nat Med 2020 Jul 11;26(7):1037-1040 [FREE Full text] [doi: 10.1038/s41591-020-0916-2] [Medline: 32393804]
18. Rossman H, Keshet A, Shilo S, Gavrieli A, Bauman T, Cohen O, et al. A framework for identifying regional outbreak and spread of COVID-19 from one-minute population-wide surveys. Nat Med 2020 May;26(5):634-638 [FREE Full text] [doi: 10.1038/s41591-020-0857-9] [Medline: 32273611]
19. Drew DA, Nguyen LH, Steves CJ, Menni C, Freydin M, Varsavsky T, COPE Consortium. Rapid implementation of mobile technology for real-time epidemiology of COVID-19. Science 2020 Jun 19;368(6497):1362-1367 [FREE Full text] [doi: 10.1126/science.abc0473] [Medline: 32371477]
20. Kreuter F. Partnering with a global platform to inform research and public policy making. Surv Res Methods 2020;14(2):159-163. [doi: 10.18148/srm/2020.v14i2.7761]

21. Wang C, Han L, Stein G, Day S, Bien-Gund C, Mathews A, et al. Crowdsourcing in health and medical research: a systematic review. Infect Dis Poverty 2020 Jan 20;9(1):8 [FREE Full text] [doi: 10.1186/s40249-020-0622-9] [Medline: 31959234]
22. Post J, Class F, Kohler U. Unit nonresponse biases in estimates of SARS-CoV-2 prevalence. Surv Res Methods 2020;14(2):115-121. [doi: 10.18148/srm/2020.v14i2.7755]
23. Klingwort J, Schnell R. Critical limitations of digital epidemiology: why COVID-19 apps are useless. Surv Res Methods 2020;14(2):95-101. [doi: 10.18148/srm/2020.v14i2.7726]
24. Bendavid E, Mulaney B, Sood N, Shah S, Bromley-Dulfano R, Lai C, et al. COVID-19 antibody seroprevalence in Santa Clara County, California. Int J Epidemiol 2021 May 17;50(2):410-419 [FREE Full text] [doi: 10.1093/ije/dyab010] [Medline: 33615345]
25. Schaurer I, Weiß B. Investigating selection bias of online surveys on coronavirus-related behavioral outcomes. Surv Res Methods 2020;14(2):103-108. [doi: 10.1007/978-3-030-39903-0_301696]
26. Textor J, van der Zander B, Gilthorpe MS, Liskiewicz M, Ellison GT. Robust causal inference using directed acyclic graphs: the R package 'dagitty'. Int J Epidemiol 2016 Dec 01;45(6):1887-1894. [doi: 10.1093/ije/dyw341] [Medline: 28089956]
27. Chunara R, Chhaya V, Bane S, Mekaru SR, Chan EH, Freifeld CC, et al. Online reporting for malaria surveillance using micro-monetary incentives, in urban India 2010-2011. Malar J 2012 Feb 13;11:43 [FREE Full text] [doi: 10.1186/1475-2875-11-43] [Medline: 22330227]
28. Walters K, Christakis DA, Wright DR. Are Mechanical Turk worker samples representative of health status and health behaviors in the U.S.? PLoS One 2018;13(6):e0198835 [FREE Full text] [doi: 10.1371/journal.pone.0198835] [Medline: 29879207]
29. Chan C, Holosko MJ. An overview of the use of Mechanical Turk in behavioral sciences. Res Soc Work Pract 2015 Jul 06;26(4):441-448. [doi: 10.1177/1049731515594024]
30. Mason W, Suri S. Conducting behavioral research on Amazon's Mechanical Turk. Behav Res Methods 2012 Mar;44(1):1-23. [doi: 10.3758/s13428-011-0124-6] [Medline: 21717266]
31. Ophir Y, Sisso I, Asterhan CSC, Tikochinski R, Reichart R. The Turker blues: hidden factors behind increased depression rates among Amazon’s Mechanical Turkers. Clin Psychol Sci 2019 Oct 02;8(1):65-83. [doi: 10.1177/2167702619865973]
32. Office of the Governor of New Jersey. Governor Murphy Announces Statewide Stay at Home Order, Closure of All Non-Essential Retail Businesses. URL: https://www.nj.gov/governor/news/news/562020/20200320j.shtml [accessed 2022-02-26]
33. Office of Governor of New York State. Governor Cuomo Signs the “New York State on PAUSE” Executive Order. URL: https://www.governor.ny.gov/news/governor-cuomo-signs-new-york-state-pause-executive-order [accessed 2022-02-26]
34. New York City Department of Health and Mental Hygiene. 2020 Health Alert #4 : COVID-19 Updates for New York City. URL: https://www1.nyc.gov/assets/doh/downloads/pdf/han/alert/2020/covid-19-update-030920.pdf [accessed 2022-02-26]
35. New York City Department of Health and Mental Hygiene. 2020 Health Alert #6 : COVID-19 Updates for New York City. URL: https://www1.nyc.gov/assets/doh/downloads/pdf/han/alert/2020/covid-19-03152020.pdf [accessed 2022-02-26]
36. New York City Department of Health and Mental Hygiene. 2020 Health Alert #8 : COVID-19 Update for New York City. URL: https://www1.nyc.gov/assets/doh/downloads/pdf/han/advisory/2020/covid-19-03202020.pdf [accessed 2022-02-26]
37. New York State Department of Health. Health Advisory : COVID-19 Update for Local Health Department Response Activities. URL: https://coronavirus.health.ny.gov/system/files/documents/2020/04/doh_covid19_lhdupdate_040720.pdf [accessed 2022-02-26]
38. New York State Department of Health. 2019 Novel Coronavirus (COVID-19) Interim Guidance: Protocol for COVID-19 Testing Applicable to All Health Care Providers and Local Health Departments. 2019. URL: https://coronavirus.health.ny.gov/system/files/documents/2020/04/doh_covid19_revisedtestingprotocol_042620.pdf [accessed 2022-02-26]
39. New Jersey Department of Health. Surveillance Criteria and Testing for Novel Coronavirus 2019 (COVID-19). URL: https://www.nj.gov/health/cd/documents/topics/NCOV/Surveillance [accessed 2022-02-26]
40. Bajema KL, Wiegand RE, Cuffe K, Patel SV, Iachan R, Lim T, et al. Estimated SARS-CoV-2 seroprevalence in the US as of September 2020. JAMA Intern Med 2021 Apr 01;181(4):450-460 [FREE Full text] [doi: 10.1001/jamainternmed.2020.7976] [Medline: 33231628]
41. Thompson CN, Baumgartner J, Pichardo C, Toro B, Li L, Arciuolo R, et al. COVID-19 outbreak - New York City, February 29-June 1, 2020. Morb Mortal Wkly Rep 2020 Nov 20;69(46):1725-1729 [FREE Full text] [doi: 10.15585/mmwr.mm6946a2] [Medline: 33211680]
42. Yang W, Kandula S, Huynh M, Greene SK, Van Wye G, Li W, et al. Estimating the infection-fatality risk of SARS-CoV-2 in New York City during the spring 2020 pandemic wave: a model-based analysis. Lancet Infect Dis 2021 Feb;21(2):203-212 [FREE Full text] [doi: 10.1016/S1473-3099(20)30769-6] [Medline: 33091374]
43. Meyerowitz-Katz G, Merone L. A systematic review and meta-analysis of published research data on COVID-19 infection fatality rates. Int J Infect Dis 2020 Dec;101:138-148 [FREE Full text] [doi: 10.1016/j.ijid.2020.09.1464] [Medline: 33007452]
44. Bradley VC, Kuriwaki S, Isakov M, Sejdinovic D, Meng X, Flaxman S. Unrepresentative big surveys significantly overestimated US vaccine uptake. Nature 2021 Dec;600(7890):695-700 [FREE Full text] [doi: 10.1038/s41586-021-04198-4] [Medline: 34880504]

Abbreviations

ACS: American Community Survey
DAG: directed acyclic graph
HIT: human intelligence task
ILI: influenza-like illness
MTurk: Mechanical Turk
NJ/NY: New Jersey and New York
NYC: New York City
NYC CBSA: New York City Combined Statistical Area contained within New Jersey and New York
rRT-PCR: real-time reverse transcription polymerase chain reaction

Edited by T Sanchez; submitted 16.06.21; peer-reviewed by N Hozé, M Bestek, R Poluru; comments to author 04.11.21; revised version received 22.02.22; accepted 17.05.22; published 21.07.22

Please cite as:
Stockham N, Washington P, Chrisman B, Paskov K, Jung JY, Wall DP
Causal Modeling to Mitigate Selection Bias and Unmeasured Confounding in Internet-Based Epidemiology of COVID-19: Model Development and Validation
JMIR Public Health Surveill 2022;8(7):e31306
URL: https://publichealth.jmir.org/2022/7/e31306
doi: 10.2196/31306
PMID: 35605128